Sensors and Materials, Vol. 34, No. 6 (2022) 2053–2064
MYU Tokyo

S & M 2955

Electrical Properties of Spin-coated Indium Tin Oxide for Photosensor Applications

Shih-Chen Shi,[1*] Jian-An Chen,[1] Yue-Feng Lin,[2] and Chih-Chia Wang[3,4]

[1]Department of Mechanical Engineering, National Cheng Kung University,
No. 1, University Road, Tainan City 70101, Taiwan
[2]Department of Mechanical Engineering, National Chin-Yi University of Technology,
No. 57, Sec. 2, Zhongshan Rd., Taiping Dist., Taichung 411030, Taiwan
[3]Department of Chemical and Materials Engineering, Chung Cheng Institute of Technology,
National Defense University, Taoyuan 33509, Taiwan
[4]Undergraduate Degree Program of System Engineering and Technology,
National Yang Ming Chiao Tung University, Hsinchu 30010, Taiwan

(Received December 20, 2021; accepted May 10, 2022)

Keywords: indium tin oxide, spin-coating, sensor

A high-performance indium tin oxide (ITO) coating is key in fabricating an efficient photosensor. The manufacturing process of ITO is complex and time-consuming. Therefore, establishing a production technology that is fast and capable of application to large areas is essential. The dispersion of nanoparticles in the process has a considerable influence on the photoelectric properties of ITO films. The degree of dispersion also determines the existence of the secondary phase, which is harmful during application. In this study, we compared the effect of different dispersion parameters such as the ultrasonic power and type of dispersant on the properties of spin-coated ITO films, i.e., the interfacial zeta potential, extinction ratio, and electrical properties. The electrical properties of spin-coated ITO films were affected by oxygen vacancies and the uniformity of tin oxide doping. Using an ultrasonic crusher with an output power of 600 W (3 h) with D305 dispersant, we obtained ITO particles with a minor hydrodynamic diameter of 176 nm. The spin-coated ITO film comprising these particles had a resistivity of as low as 10^{-4} Ω·cm after suitable heat treatment and a carrier concentration of approximately 10^{20} cm^{-3}. The electrical properties of the spin-coated ITO were satisfactory for its application on a photodetector. Finally, we proposed that the service life of a sensor can be evaluated by monitoring the variation of the friction coefficient.

1. Introduction

Recent new applications for photosensors include medical uses,(1) imaging,(2) communications,(3) and automatic control,(4) and they are of particular importance as optoelectronic devices. Transparent conductive films (TCFs) are widely used in photodetector applications.(5) The characteristics of the TCF also determine the performance of the photoelectric element. There are many types of TCFs, which are mainly oxide films. A TCF

*Corresponding author: e-mail: scshi@mail.ncku.edu.tw
https://doi.org/10.18494/SAM3782

ISSN 0914-4935

must have a penetration rate of 80% and a resistance of less than 10^{-4} Ω·cm in the visible region of the electromagnetic spectrum (380–780 nm). Currently, indium tin oxide (ITO) is the most commonly used TCF and has low resistivity and good transmittance of visible light.

ITO is a binary material, making the even mixing of heterogeneous materials necessary. Tin oxide has a larger particle size and higher precipitation speed than indium oxide. The ultrasonic processing time and power are key parameters in the processing of ITO and must be studied; the optimization of these parameters can reduce the average particle size of the slurry. ITO nanoparticles, a reduced precipitation rate, and small agglomerations of ITO can be obtained through space steric hindrance and electric space steric hindrance by applying an electric double layer of ionic and non-ionic dispersants. The high dispersion stability of slurry also means that the average hydrodynamic diameter of particles in the colloidal system is small, the precipitation rate is low, and the particles are packed tightly after extrusion. As a result, the microstructure of the ceramic crystal phase is homogeneous, the number of internal defects is low, and the relative density is high.[6,7] Reducing the average particle size of a suspension and increasing the extinction ratio of tin oxide can increase the homogeneity of tin oxide doping, thereby forming a solid solution after sintering into a target. A well-mixed slurry allows the formation of a homogeneous secondary phase in the target. This phase reduces the number of internal pores, increases the relative density, and stabilizes the quality of a physical vapor deposition coating.[6] This phase also reduces the number of nodules on the target surface after prolonged sputtering, stabilizes the production capacity, and maintains the film quality, thereby reducing material and electricity wastage.

With the aim of maintaining the characteristics of nanoparticles and ensuring the homogeneous mixing of multiple materials, many colloidal studies have been carried out to stably disperse nanoparticles in different solvents (including water and ethanol) as dispersion media to form nanosuspensions. In colloidal systems, nanoparticles are in a dispersed phase. They are impacted by molecules in the solvent, resulting in irregular thermal motion known as Brownian motion, which increases as the particle size and the viscosity of the dispersed system decrease and the temperature of the system rises. Particles collide because their van der Waals or Coulomb forces cause flocculation or aggregation. The former is caused by the weak van der Waals bonding force, whereas a strong chemical bonding force causes the latter, and the aggregate cannot be redispersed via ultrasonic treatment. Therefore, the hydrodynamic diameter of the nanoparticles in the dispersion system will be larger than the first-order particle size.[8] To maintain the long-term stability of a nanoparticle suspension, dispersants or surfactants are applied to the dispersant system to prevent aggregation caused by particle absorption. Ammonium polyacrylate (APA) and diammonium citrate (DAC), which are both carboxylic surfactants, disperse yttria-stabilized zirconia.[9] The carboxylic group is negatively charged after dissociation, and the adsorption capacity of the carboxylic group is more vital than that of OH. The dissociated dispersant chain segments are adsorbed on the particle surface through the carboxylic groups.[10]

Nanoparticles have a high specific surface area and rapidly form a neck during sintering, resulting in many pores in materials. Particle sliding is blocked during the compaction process. Problems such as internal layer cracking and external stripping during the compaction process

impact the quality of the sintering body. Increasing the degree of material depolymerization can increase the bulk density of particles, thereby enhancing the compactness of ceramics.[11–13]

In preprocessing before the industrial mass production of target materials, ball milling with a dispersant is used to refine particles, improve the dispersion stability of nanoparticles, uniformly mix multiple materials, increase the bulk density of materials, and improve the density of target materials after sintering. However, if the dispersion stability of a slurry is poor, then there will be more agglomeration in the preparation of a powder and large pores between particles, thereby reducing the density of the target material. In the formation of $In_4Sn_3O_{12}$, grains precipitate in the case of uneven doping. The electrical resistance of $In_4Sn_3O_{12}$ is twice that of the primary grains due to the high density of the structure.[14] Under the influence of elemental resistance, a considerable amount of charge accumulates in some areas of the target, making it prone to abnormal discharge phenomena. This leads to an increase in the film resistance, a decrease in the penetration rate, and the formation of nodules on the target surface. The nodules continuously aggravate the abnormal discharge, resulting in a reduced target sputtering rate.[6]

Utsumi *et al.* used ITO targets with relative densities of 99, 97, and 90% for experiments, deposited ITO films of 50 nm thickness by physical vapor deposition, and obtained resistivities of 149, 159, and 161 μΩ·cm, respectively.[15] Nakashima and Kumahara improved the powder mixing technology, improved the dispersion of tin oxide in indium oxide, increased the density of the ITO target, and reduced the formation of nodules on the target surface. After sputtering at 160 Wh/cm^2, they compared the appearance of the targets and recorded the number of abnormal discharges generated during sputtering.[6]

By adding tin oxide to indium oxide, free electrons are provided through the tetravalent cations (Sn^{4+}). An n-type semiconductor can effectively reduce the resistivity of ITO films. Ohya *et al.* doped ITO targets with 2, 3.5, and 7 at.% SnO_2 and sintered them in an oxygen atmosphere at 1300, 1400, and 1500 °C, respectively. They used X-ray diffraction to compare the secondary phase formation of ITO targets for different doping levels.[16] Mei *et al.* prepared an ITO target with a 90:10 mass ratio and sintered it at 1580 °C for 10 h and 1600 °C for 5 h to obtain targets A and B with relative densities of 99.79 and 99.75%, respectively. After etching, they compared the secondary phase grain size of the two targets.[17] Medvedovski *et al.* prepared ITO targets with weight ratios of 90:10 and 80:20. When the doping of tin oxide was above 7 at.%, secondary phase grains began to form, and the grain size increased with increasing doping. Owing to the high density of the secondary phase, the relative density and strength of the target were positively correlated. The opposite was true for the resistivity of the target.[18]

The traditional sintering process has been unable to meet the needs of large-area transparent conducting oxides (TCOs). Therefore, large-scale processes are being actively developed for the deposition of TCO films. These processes include the sol-gel and spray methods.[19,20] However, the conversion process of the metal compound/precursor will generate other structures.

According to the above references, there is a positive correlation between the electrical properties of ITO and the sintering density of the target material. Simultaneously, the sintering density of the target material is positively correlated with the particle size and the dispersion of its components. However, ITO manufacturing is a complicated process, involving green body formation, target sintering, and sputtering, which require considerable time. Therefore, we take

ITO powder as the starting point, disperse it using an ultrasonic wave, and then process the resulting ITO film by spin-coating. This ITO film production process is fast and applicable to large areas. Subsequently, the electrical properties of the spin-coated films were analyzed to establish the correlation between the dispersion of the nanoparticles and the properties of the ITO. Finally, a fast validation method was proposed to evaluate the ITO film quality.

2 Materials and Methods

2.1 Slurry preparation and characteristics analysis

High-purity indium oxide and tin oxide nanoparticles (SOLAR, Tainan City, Taiwan) with hexagonal wurtzite crystal and rutile tetragonal structures and diameters of 58 ± 7 and 123 ± 28 nm, respectively, were used. An ultrasonic disintegrator (DC300H, Delta Ultrasonic Co., Ltd., Taiwan) was used to mix the ITO nanoparticles. D305, diammonium citrate (DAC), dodecyl trimethylammonium bromide (DTAB), polyvinylpyrrolidone (PVP), and polyethylene glycol (PEG) were used as dispersants. The hydrodynamic diameter of the suspension was measured by dynamic light scattering (DLS; Delsa Nano C, Beckman Coulter, Brea, USA). An interfacial potential analyzer (ZETAPROBE ANALYZER™, Colloidal Dynamics, MA, USA) was used to analyze the zeta potential, dynamic mobility, and isoelectric point of the slurry. A UV–visible–near-IR reflectance spectrophotometer (U.V. Solution 2900, HITACHI, Japan) was used to detect the extinction ratio.

2.2 Spin-coating and thin-film characterization

A micropipette was used to inject 500 μL of slurry onto a glass substrate (Corning, USA). The substrate was fixed to a spin coater (Hong Yu Instrument Co. Ltd., Taichung, Taiwan). The substrate was first subjected to rotation at 3000 rpm for 30 s and then to rotation at 5000 rpm for 3 s. Subsequently, we placed the spin-coated ITO in a furnace with argon gas with a pressure of 60 mTorr and a temperature of 700 °C for 20 h. The electrical properties of the films were obtained using a Hall effect measurement system (AHM-800B, Agilent Technologies, Santa Clara, CA, USA).

2.3 Tribology behavior of spin-coated ITO

The tribological performances of the spin-coated ITO were measured using a ball-disk friction and wear tester (POD-FM406-10NT, Fu Li Fong Precision Machine, Kaohsiung, Taiwan). The load was 2 N, the rotating diameter was 10 mm, the sliding speed was 0.03 m/s, and the friction distance was 100 m. All tribological experiments were carried out in a laboratory with controlled temperature (20 °C) and relative humidity (50%) The friction coefficients were monitored and recorded by sensors in real time. In addition, the wear diameter was measured with a 3D laser scanner (VK9700, Keyence, Osaka, Japan). The upper ball used in the tribological experiments was a copper ball (C66400), and the lower disk was the spin-coated ITO film.

3. Results and Discussion

3.1 Characterization of ITO slurry

The particle size distribution of the slurry after ball milling was analyzed (dispersant: D305). The average hydrodynamic diameters of indium oxide and tin oxide particles were 224.3 and 218.0 nm, respectively, as shown in Fig. 1. In subsequent experiments, the direct ultrasonic

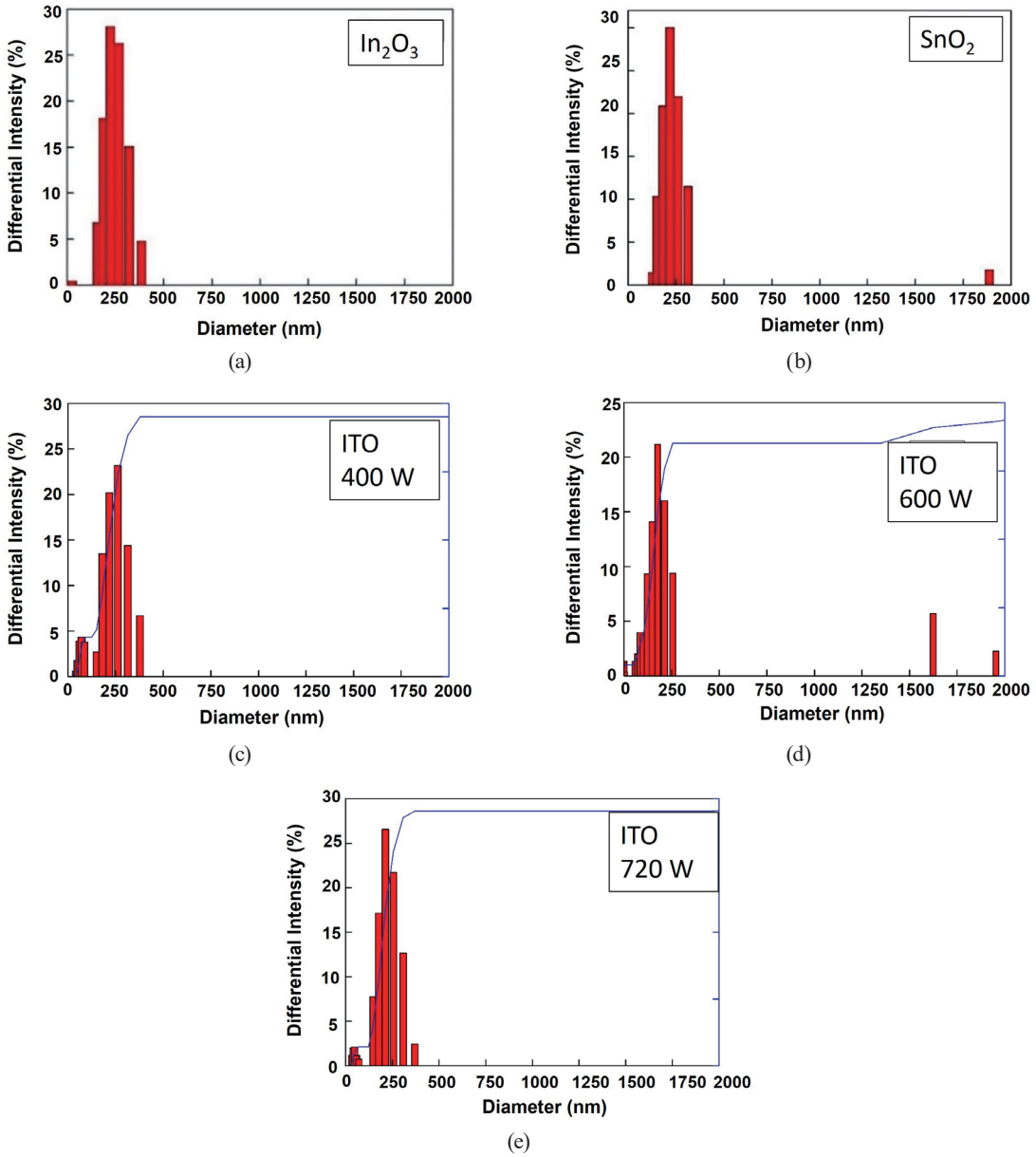

Fig. 1. (Color online) Hydrodynamic diameter distributions of particles in fresh (a) In_2O_3 slurry and (b) SnO_2 slurry, and distributions of nanoparticle size in ITO slurry after 3 h of sonication treatment at (c) 480 W, (d) 600 W, and (e) 720 W.

method was used to disperse nanoparticles, and the output power and oscillation time were adjusted to minimize the liquid motion of the ITO slurry. The ultrasonic wave disperses the nanoparticles by the shockwave generated by the collapse of cavitation bubbles. The higher the output power, the higher the temperature of the slurry we obtained. A high-temperature slurry led to greater thermal motion and agglomeration of the nanoparticles. Therefore, the output power of the ultrasonic wave used for particle dispersion was set to 480, 600, and 720 W. The average hydrodynamic diameters of ITO slurry particles for these output powers, analyzed by DLS, were 191.0, 176.0, and 191.2 nm, respectively, which were much lower than that of the ball-milled slurry. Therefore, the average particle size was effectively reduced when the output power was increased from 480 to 600 W. However, when the output power was increased to 720 W, the cooling equipment could not maintain the slurry at a stable temperature. The intensified thermal motion increased particle collisions and the average hydrodynamic particle diameter, as shown in Figs. 1(c) and 1(d). The subsequent experiments were conducted with an output power of 600 W used for nanoparticle dispersion.

The influence of the type and amount of dispersant on the average hydrodynamic diameter and the median (D_{50}) of the particle size distribution is shown in Table 1. Ionic dispersants such as D305, DAC, and DTAB induce bridging mechanisms, which increase the average hydrodynamic diameter of suspensions and lead to the agglomeration and sedimentation of nanoparticles. Smaller amounts of additives result in better dispersion stability.

Table 1
Relation between type and amount of dispersant and particle size of suspension.

Dispersant	Additive amount (wt.%)	DLS particle size (nm)	D_{50} (nm)
D305	0.1	2105.9	1376.3
	0.5	253.1	200.1
	1	176.0	216.3
	2	252.7	327.4
DAC	0.1	4393.3	3923.3
	0.5	279.7	243.4
	1	131.0	124.6
	2	248.5	255.7
DTAB	0.1	239.2	227.5
	0.5	255.4	249.7
	1	279.2	237.2
	2	984.3	556.9
PEG	10	1638.4	1901.1
	50	440.0	324.9
	100	306.2	376.7
	120	356.4	302.3
	140	285.4	291.9
	200	328.1	385.2
PVP	10	307.5	254.9
	50	370.8	277.1
	100	473.3	537.8
	200	557.6	617.3

The zeta potential of the ITO slurry with different dispersants was measured at different pH values, as shown in Fig. 2. The isoelectric point of pure ITO was approximately pH 7. After adding cationic DTAB dispersant, the isoelectric point shifted in the alkaline direction (to around pH 9). The zeta potential of DTAB-ITO was high in the pH range of 3–5, meaning that DTAB-ITO is well dispersed in an acidic environment. DAC and D305 are anionic dispersants with a good synergy effect with indium oxide and tin oxide in the pH range of 3–11, resulting in a high zeta potential. With the addition of anionic dispersants (DAC and D305), the zeta potential of the ITO slurry could be maintained at a stable value (pH 4–11). This stable and significant value (absolute value >20) indicated that indium oxide and tin oxide were well dispersed in the solution. Meanwhile, high dispersibility regardless of the pH can improve flexibility in practical manufacturing processes.

The extinction ratio was obtained by measuring the sample absorbance (A) with UV–Vis light every 10 min and dividing it by the initial absorbance (A_0). The greater the extinction ratio, the greater the absorption of the sample, indicating that the suspended particles remained in the slurry. The nanoparticles in the suspension gradually precipitated over time, and the absorption intensity of the measured sample decreased, resulting in a decrease in the extinction ratio. The average hydrodynamic diameter and D_{50} of the nanoparticles dispersed with DAC and D305 were similar; thus, the extinction ratio trend of the ITO slurry was similar for these dispersants, as shown in Fig. 3. The absolute zeta potential of the dispersant-ITO between 40 and 60 mV indicated a suspension with good dispersion. However, this slurry is still affected by the surface dissociation of nanoparticles, chain segments in the dispersant, and the ionic strength of the solution. D305 and DAC have molar masses of 6000 and 226 g/mol, respectively. The dispersant has a high molar mass and long molecular chains, enhancing the bridging effect between particles and resulting in the agglomeration of nanoparticles.[21] The smaller the particle size, the lower the precipitation rate, resulting in a high extinction ratio and high dispersion stability.

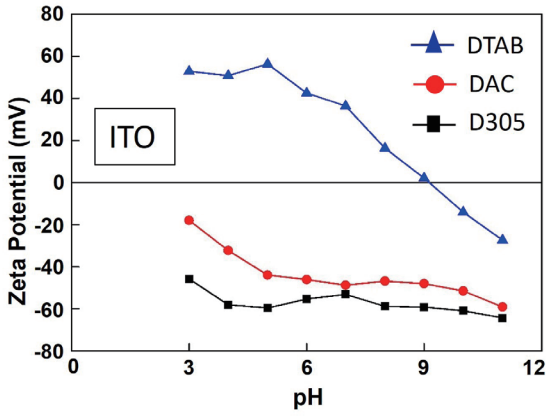

Fig. 2. (Color online) Zeta potential results of ITO slurry with various dispersants.

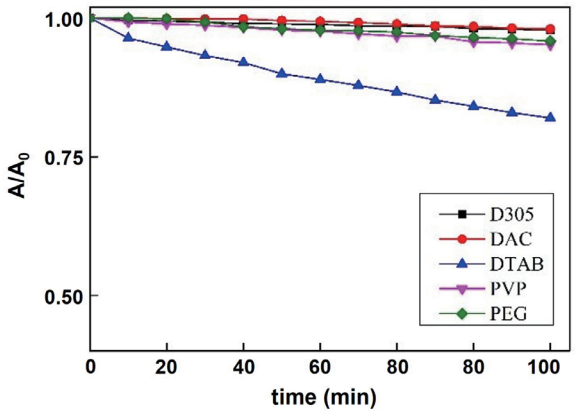

Fig. 3. (Color online) Extinction ratio results of ITO slurry with various dispersants.

3.2 Characterization of spin-coated ITO

The ITO suspension was used for spin-coating. The cross section of the resulting film was observed by SEM and the thickness of the film was measured. Among the dispersants, D305 and DAC had the highest dispersion stability, resulting in the formation of a continuous and uniform film on the substrate. The DTAB, PEG, and PVP pastes had many agglomerates with poor affinity to the substrate, and discontinuous films were formed after spin-coating. The SEM images in Figs. 4(c)–4(e) show that many agglomerates attached to the film surface.

As shown in Fig. 4, the films of the D305 and DAC spin-coated slurries on the substrate were thinnest among the dispersants, with fewest aggregates in the slurry, and the films were uniform and continuous. The DTAB slurry caused the nanoparticles to quickly agglomerate and settle in the slurry. After spin-coating on the substrate, there were many large, agglomerated particles, and the film showed discontinuity, thus increasing its resistivity. The PEG and PVP films had many large agglomerated particles on the surface, the film thickness was not uniform, and the films were discontinuous, resulting in high resistance. The electrical properties of the films for the different dispersants are shown in Table 2.

3.3 Tribology behavior of spin-coated ITO

There is high affinity between the glass substrate and the D305 and DAC, and the films are uniform and continuous. DTAB-, PEG-, and PVP-ITO are discontinuous films owing to the many agglomerates in the slurry, and ITO was attached to the substrate in the form of large agglomerates. The influence of the dispersants on the uniformity and dispersion of ITO thin films can be seen in Fig. 4.

We next evaluated the ease of removing the ITO films with different dispersants by grinding using copper balls. The thin ITO films with poor dispersion were easy to remove by grinding owing to the numerous large agglomerated particles on the film surface. As a result, only a few ITO particles participated in the grinding process, resulting in the low wear of the copper balls.

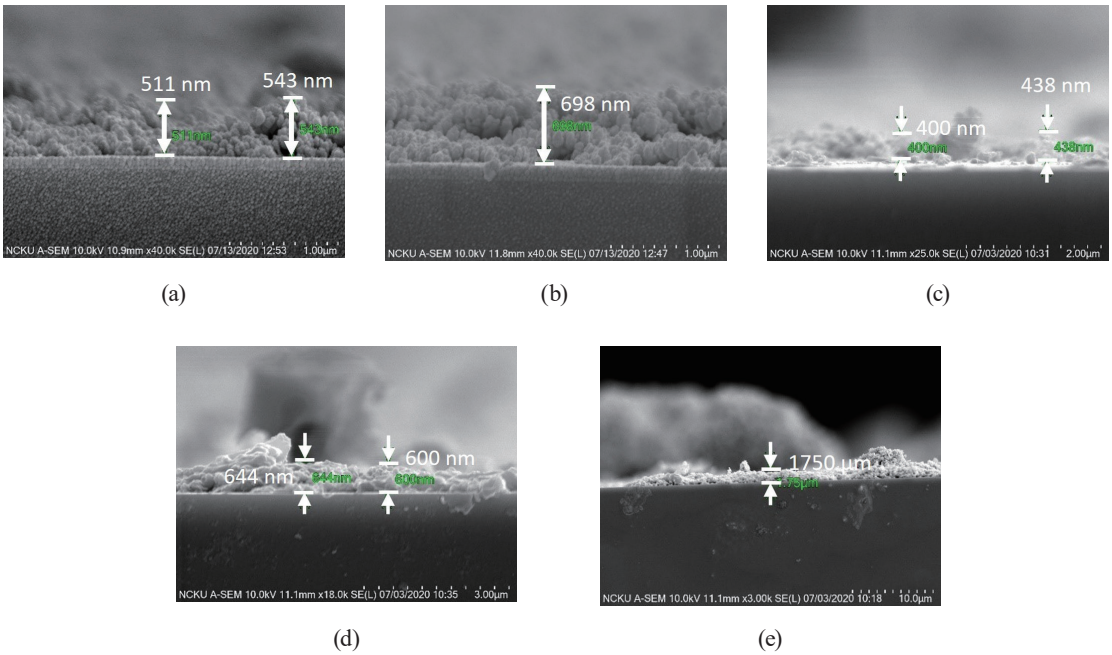

Fig. 4. (Color online) Cross-sectional SEM images of films obtained using (a) D305, (b) DAC, (c) DTAB, (d) PEG, and (e) PVP dispersants.

Table 2
Electrical properties of the ITO films for different dispersants.

Sample	DLS particle size (nm)	Resistivity (Ω·cm)	Carrier concentration (cm^{-3})
D305	176.0	9.10×10^{-3}	5.85×10^{19}
DAC	131.0	1.97×10^{-2}	8.57×10^{19}
DTAB	239.2	6.64×10^{-1}	1.67×10^{18}
PEG	285.4	5.80×10^{4}	8.76×10^{11}
PVP	557.6	3.84×10^{4}	3.10×10^{10}

The friction coefficients of the poorly dispersed ITO films (DTAB-, PEG-, and PVP-ITO) were close to that of a pure glass substrate. The friction coefficient of a glass substrate increases with increasing wear distance due to the increased contact area. With increasing wear distance, the number of ITO particles between the copper balls and the glass substrate becomes smaller than that between the thin films with a poor dispersion, leaving a large area of wear on the surface of the copper balls as shown in Fig. 5. The influence of the dispersant properties on the wear of copper balls is shown in Table 3. The more well-dispersed ITO slurries have a smaller DLS particle size. Therefore, the spin-coating process enables the preparation of a high-quality ITO film with good anti-wear properties. Figure 5 shows the wear diameter of the copper ball for each dispersant, where a larger wear diameter indicates a harder ITO film. A hard ITO film causes wearing of the copper ball, and the copper chips that are removed as a result of wear remain in the friction interface, producing a lubricating effect and reducing the friction coefficient.

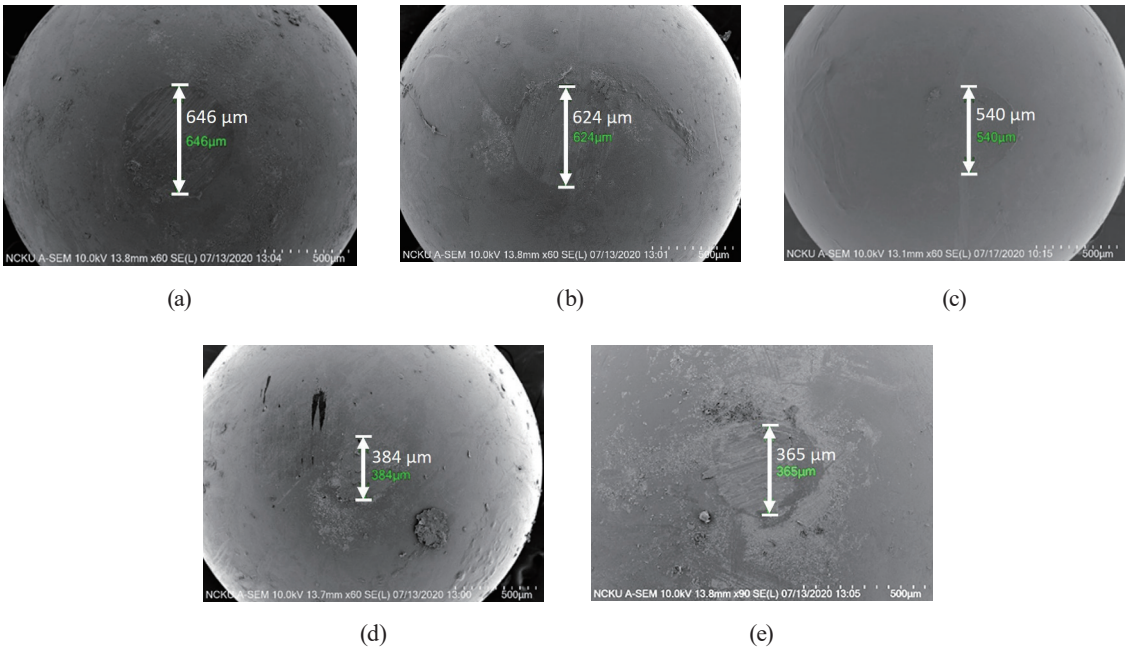

Fig. 5. Surface morphology and wear diameter of Cu ball for different dispersants: (a) D305, (b) DAC, (c) DTAB, (d) PEG, and (e) PVP.

Table 3
Effect of dispersant on wear diameter of copper ball.

Sample	DLS particle size (nm)	Wear diameter (µm)	Friction coefficient
Glass	—	—	0.113
D305	176.0	603	0.197
DAC	131.0	624	0.206
DTAB	239.2	540	0.144
PEG	285.4	384	0.140
PVP	557.6	365	0.121

4. Conclusions

Among the dispersants considered in this study, D305 had the best dispersion effect. After 3 h of ultrasonic treatment, the average hydrodynamic diameter of nanoparticles dispersed with D305 was reduced from 218 to 176 nm. Experimental results showed that the ITO surface was more uniform when the average hydrodynamic diameter was smaller. Moreover, through the rapid verification of the extinction ratio, we found that superior film characteristics, including film uniformity, density, and conductivity, were obtained with a well-dispersed slurry. The homogeneous and dense spin-coated ITO films in this study had good anti-wear characteristics and caused severe wear on copper balls. The low-density ceramic and copper chips embedded in the ITO film provide lubrication, resulting in a low friction coefficient. Because the friction coefficient decreases as the ITO undergoes wear, the friction coefficient can be used as an evaluation index for the quality and lifetime of ITO.

Acknowledgments

This work was supported by the Ministry of Science and Technology, Taiwan (grant number MOST 110-2221-E-006-150).

References

1 F. Bandi, V. Ilisie, I. Vornicu, R. Carmona-Galán, J. M. Benlloch, and Á. Rodríguez-Vázquez: Sensors **22** (2022) 122. https://doi.org/10.3390/s22010122
2 J. Kim, C. Jo, M. G. Kim, G. S. Park, T. J. Marks, A. Facchetti, and S. K. Park: Adv. Mater. **34** (2022) 2106215. https://doi.org/10.1002/adma.202106215
3 P. Grybos, R. Kleczek, P. Kmon, A. Krzyzanowska, P. Otfinowski, R. Szczygiel, and M. Zoladz: J. Instrum. **17** (2022) C01036. https://doi.org/10.1088/1748-0221/17/01/C01036
4 Y. Zhang and M. Liu: J. Nanoelectron. Optoelectron. **16** (2021) 324. https://doi.org/10.1166/jno.2021.2960
5 Y. Zhao and K. Zhu: Chem. Soc. Rev. **45** (2016) 655. https://doi.org/10.1039/C4CS00458B
6 K. Nakashima and Y. Kumahara: Vacuum **66** (2002) 221. https://doi.org/10.1016/S0042-207X(02)00145-8
7 B.-C. Kim, J.-H. Lee, J.-J. Kim, and T. Ikegami: Mater. Lett. **52** (2002) 114. https://doi.org/10.1016/S0167-577X(01)00377-9
8 J. Jiang, G. Oberdörster, and P. Biswas: J. Nanopart. Res. **11** (2009) 77. https://doi.org/10.1007/s11051-008-9446-4
9 P. Sinaga and S.-H. Bae: Adv. Mater. Sci. Eng. **28** (2018) 2965137. https://doi.org/10.1155/2018/2965137
10 F. Zerafati, H. Majidian, and L. Nikzad: Adv. Ceramics Prog. **5** (2019) 15. https://doi.org/10.2298/PAC2002154Z
11 H. Ferkel and R. Hellmig: Nanostruct. Mater. **11** (1999) 617. https://doi.org/10.1016/S0965-9773(99)00348-7
12 L. Wu, M.-C. Chure, K.-K. Wu, W.-C. Chang, M.-J. Yang, W.-K. Liu, and M.-J. Wu: Ceram. Intl. **35** (2009) 957. https://doi.org/10.1016/j.ceramint.2008.04.030
13 B. V. Velamakanni and F. F. Lange: J. Am. Ceram. Soc. **74** (1991) 166. https://doi.org/10.1111/j.1151-2916.1991.tb07313.x
14 G. P. Crawford: Flexible Flat Panel Displays (John Wiley & Sons Ltd, Chichester, 2005) p. 1.
15 K. Utsumi, O. Matsunaga, and T. Takahata: Thin Solid Films **334** (1998) 30. https://doi.org/10.1016/S0040-6090(98)01111-0
16 Y. Ohya, T. Ito, M. Kaneko, T. Ban, and Y. Takahashi: J. Ceram. Soc. Jpn. **108** (2000) 803. https://doi.org/10.2109/jcersj.108.1261_803
17 F. Mei, T. Yuan, and R. Li: Ceram. Intl. **43** (2017) 8866. https://doi.org/10.1016/j.ceramint.2017.04.021
18 E. Medvedovski, N. Alvarez, O. Yankov, and M. Olsson: Ceram. Intl. **34** (2008) 1173. https://doi.org/10.1016/j.ceramint.2007.02.015
19 H. Taha, K. Ibrahim, M. M. Rahman, D. J. Henry, C.-Y. Yin, J.-P. Veder, A. Amri, X. Zhao, and Z.-T. Jiang: Appl. Surface Sci. **530** (2020) 147164. https://doi.org/10.1016/j.apsusc.2020.147164
20 S.-C. Shi, P.-W. Huang, and J. H.-C. Yang: Coatings **11** (2021) 1001. https://doi.org/10.3390/coatings11081001
21 S. Farrokhpay: Adv. Colloid Interface Sci. **151** (2009) 24. https://doi.org/10.1016/j.cis.2009.07.004

About the Authors

Shih-Chen Shi received his B.S. and M.S. degrees from National Cheng Kung University, Taiwan, in 1999 and 2001, respectively, and his Ph.D. degree from National Chiao Tung University, Taiwan, in 2005. From 2007 to 2012, he was the head of the R&D Department at Everlight Electronic Co., Ltd., Taiwan. Since 2019, he has been an associate professor at National Cheng Kung University. His research interests include nanomaterials, tribology, LED applications, and sustainable materials. (scshi@mail.ncku.edu.tw)

Jian-An Chen received his M.S. degree from National Cheng Kung University in 2020.

Yue-Feng Lin received his B.S., M.S., and Ph.D. degrees from National Cheng Kung University, Taiwan, in 2008, 2009, and 2016, respectively. From 2017 to 2018, he was a postdoctoral researcher at National Chung Hsing University, Taiwan. Since 2018, he has been an assistant professor at National Chin-Yi University of Technology, Taiwan. His main research areas include the application of ultrasonic-vibration-assisted non-traditional processing methods to ceramic, hard, and brittle materials. (yflin@ncut.edu.tw)

Chih-Chia Wang received his B.S. and M.S. degrees from Chung Cheng Institute of Technology, National Defense University, Taiwan, R.O.C., in 2004 and 2011, respectively, and his Ph.D. degree from National Taiwan Normal University, Taiwan, R.O.C., in 2017. Since 2017, he has been an assistant professor at Chung Cheng Institute of Technology, National Defense University. His research interests are in catalytic reactions, nanomaterials, sensors and micro analysis systems, and environmental analysis.